Deep Artifact Suppression for Spiral Real-Time Phase Contrast Cardiac Magnetic Resonance Imaging in Congenital Heart Disease

Olivier Jaubert[1,2], Jennifer Steeden[2], Javier Montalt-Tordera[2], Simon Arridge[1], Grzegorz Tomasz Kowalik[2*], Vivek Muthurangu[2*]

[1.] Department of Computer Science, University College London, London. WC1E 6BT. United Kingdom

[2.] Centre for Cardiovascular Imaging, Institute of Cardiovascular Science, University College London, London. WC1N 1EH. United Kingdom

* Authors contributed equally to this study

Short Title: Deep artifact suppression for real-time spiral PCMR.

Submitted as Technical Note to Magnetic Resonance Imaging

Word count: 3108

Corresponding author:

Name	Olivier Jaubert
Department	Institute of Cardiovascular Science
Institute	University College London
Address	20c Guilford St, London WC1N 1DZ
E-mail	o.jaubert@ucl.ac.uk

Abstract

Purpose: Real-time spiral phase contrast MR (PCMR) enables rapid free-breathing assessment of flow. Target spatial and temporal resolutions require high acceleration rates often leading to long reconstruction times. Here we propose a deep artifact suppression framework for fast and accurate flow quantification.

Methods: U-Nets were trained for deep artifact suppression using 520 breath-hold gated spiral PCMR aortic datasets collected in congenital heart disease patients. Two spiral trajectories (uniform and perturbed) and two losses (Mean Absolute Error -MAE- and average structural similarity index measurement -SSIM-) were compared in synthetic data in terms of MAE, peak SNR (PSNR) and SSIM. Perturbed spiral PCMR was prospectively acquired in 20 patients. Stroke Volume (SV), peak mean velocity and edge sharpness measurements were compared to Compressed Sensing (CS) and Cartesian reference.

Results: In synthetic data, perturbed spiral consistently outperformed uniform spiral for the different image metrics. U-Net MAE showed better MAE and PSNR while U-Net SSIM showed higher SSIM based metrics.

In-vivo, there were no significant differences in SV between any of the real-time reconstructions and the reference standard Cartesian data. However, U-Net SSIM had better image sharpness and lower biases for peak velocity when compared to U-Net MAE. Reconstruction of 96 frames took ~59s for CS and 3.9s for U-Nets.

Conclusion: Deep artifact suppression of complex valued images using an SSIM based loss was successfully demonstrated in a cohort of congenital heart disease patients for fast and accurate flow quantification.

Keywords: Cardiac MRI, Congenital Heart Disease, Real time, Flow imaging, Image Reconstruction, Machine Learning.

Introduction

Flow quantification using Phase Contrast MR (PCMR) [1] is an important component of the CMR protocol in pediatric heart disease. Real-time PCMR is of particular interest in children, as it allows rapid, non-gated and free breathing flow quantification [2,3]. However, acquisition of real-time PCMR requires significant acceleration. This can be achieved using non-Cartesian trajectories [2–4] and/or data undersampling combined with state-of-the-art reconstructions such as compressed sensing (CS) [5]. Although these methods do enable accurate real-time PCMR flow quantification [4,6], long reconstruction times limit their clinical utility.

Deep learning (DL) is increasingly used for MR image reconstruction [7] and a variety of methods have been proposed, including image artifact suppression [8] and unrolled reconstruction networks [9,10]. A benefit of these methods over CS reconstructions is that computational load is shifted to training and reconstruction times are short.

A recent study applied DL image artifact suppression to radial real-time flow imaging in adults and demonstrated good image quality and accurate flow metrics [11]. Spiral trajectories have also been used for real-time PCMR, as their k-space filling efficiency enables higher spatio-temporal resolution imaging. However, DL artifact suppression may be more difficult for undersampled uniform spirals due to the presence of coherent aliasing [4]. This problem has been addressed for CS reconstructions with the use of perturbed spiral trajectories that produce more incoherent aliases [4]. This sampling pattern could also be well suited to DL approaches based on artifact suppression. The focus of this study was to develop DL artifact suppression methods for complex-valued undersampled perturbed spiral PCMR images. The specific aims were: 1) To demonstrate in synthetic PCMR data that artifact suppression of perturbed spiral images was superior to uniform density spiral images, 2) To use the trained models to perform artifact suppression in prospectively acquired perturbed spiral real-time PCMR data in children, 3) To compare flow quantification using the proposed DL models and CS reconstruction of the same real-time data, as well the reference standard Cartesian breath-hold, cardiac gated PCMR.

Methods

This study was approved by the local research ethics committee (Ref. 06/Q0508/124), and written consent was obtained in both prospective and retrospective cohorts. An overview of the proposed DL framework for real-time flow imaging is shown in Figure 1. In this study, we define U-Net augmented reconstruction as all the steps from raw k-space to the phase subtracted final image. This includes coil sensitivity estimation, non-uniform Fourier Transform, coil combination, U-Net deep artifact suppression (gridded to recovered images) of both the flow-encoded and flow-compensated data and combination to obtain the final flow maps.

Perturbed spiral design

The perturbed spiral design (Figure 1.A) has previously been described in detail [4] and has been shown to produce incoherent aliases in both space and time. Briefly, a uniform density spiral trajectory was perturbed by varying the radial acceleration as a function of both normalized distance from the k-space center and the interleave angle. In this study these interleaves were continuously rotated by the golden angle (~222º) and two interleaves were acquired per frame (with the same trajectory for flow-compensation and flow-encoding pairs). This sampling pattern was used for generation of both synthetic training data and the prospective study.

Preparation of synthetic data

The training data was created from 520 breath-hold, retrospectively cardiac gated, uniform density spiral PCMR [3] datasets in the aortic position of patients with pediatric and/or congenital heart disease (21.0 ± 13.5 years old, heart rate: 71 ± 12 bpm). Each dataset consisted of 40 combined magnitude and phase subtracted images, representing one heart-beat (acquired resolution: 1.73x1.73x6.0 mm^3) stored in the DICOM format. 490 datasets were used for training, 15 for validation and 15 for testing.

The final network needed to suppress artifact in both the uncombined flow-compensated and flow-encoded images. Thus, a smooth random additional background phase was added to simulate background offsets seen in uncombined (flow-compensated and flow-encoded) data. To obtain *truth* "real-time" images for training, the PCMR data was first interpolated to the target temporal resolution (~ 26.6 ms). A requirement for artifact suppression of real-time flow images is the ability to artifact suppress 2D+time data containing a non-integer number of heartbeats (>1) starting at any point in the cardiac cycle. Thus, the interpolated single heartbeat PCMR data was replicated over multiple heartbeats (2-4 depending on heartrate) to better reflect the prospective real-time data.

To create the paired corrupted images, the *truth* data was first Fourier transformed and undersampled with the chosen trajectory (uniform or perturbed spiral with golden angle increment and acceleration factor R~18). The synthetic undersampled k-space data was then inverse Fourier transformed to produce the aliased data (i.e. corrupted complex valued images). Both truth and corrupted images were independently normalized (divided by the maximum magnitude) and cropped to the volume size 192x192x40 centered spatially but with random start points in time (i.e. random point in the cardiac cycle and trajectory).

Network

The paired corrupted-truth images were used for supervised learning of a 3D U-Net architecture [8,12]. The input to the network consists of a 2D+time series of 18x spirally undersampled gridded images with a real and imaginary channel. The U-Net architecture (Figure 1.B) consisted of three scales separated by 2x2x2 max-pooling in the encoding branch and transpose convolutions in the decoding branch. Encoding/decoding blocks consisted of two 3D Convolutions (with 32 filters at the initial scale) and ReLU activation functions. Training was performed using an adaptive moment estimation algorithm (Adam [13]). Hyper parameters included an input/output size of 192x192x40 x2 (last dimension representing the real and imaginary channels), filter size of 3x3x3, batch size of 2 and an initial learning rate of $5x10^{-4}$. Although trained with 40 frames, at inference the network was applied to longer time-series (96 frames) to reduce artifact suppression times.

Two loss functions were investigated in this study. Mean absolute error (MAE) as proposed in other works with complex valued outputs [11,14] and a novel 3D structural similarity index [15] loss (calculated as: $1 - \mathrm{AvgSSIM}$). The average SSIM metric was adapted for complex images and is computed over the real (real) and imaginary (imag) components as follows:

$$\mathrm{AvgSSIM} = \frac{\mathrm{SSIM}\left(\frac{\mathrm{real}+1}{2}\right) + \mathrm{SSIM}\left(\frac{\mathrm{imag}+1}{2}\right)}{2} \quad (1)$$

Networks (U-Net MAE and U-Net SSIM) were trained for 100 epochs each and the best performing, as measured by the minimum loss measured on the validation dataset, were selected. Implementation and training were performed using Python (v3.7.7) and TensorFlow (v2.2.0) (24) on a Linux workstation (Ubuntu 18.08, Intel Core i9-7900X, 3.3GHz) using an NVIDIA Quadro GP100 (16GB memory).

Experiments

Synthetic data study

Four networks were trained to compare the artifact suppression quality between uniform density and perturbed spiral trajectories using both MAE and SSIM losses. The four networks were compared using synthetic data in 15 test cases through MAE, peak signal to noise ratio (PSNR), Average SSIM (AvgSSIM), Magnitude SSIM and Phase SSIM. For SSIM metrics, the background was masked using the magnitude of normalized truth images (threshold set at 0.15).

In-vivo study

The population has previously been described in the original study that described real-time perturbed spiral PCMR with CS reconstruction [4]. Briefly, 20 children (11.6 ± 3.2 years old, heart rate: 81 ± 12 bpm) referred for routine cardiac MR were scanned on an Avanto 1.5T scanner (Siemens Healthineers, Erlangen, Germany) using 2 spine coils and 1 body

matrix coil setup (total of 12 coil elements). Reference standard flow imaging was acquired using a free-breathing retrospectively ECG-gated Cartesian PCMR sequence with the following parameters - voxel-size: 1.82x1.82x6.0 mm, FOV: 350x262 mm, TR/TE: 4.4/1.9 ms, Flip Angle: 30^{o}, VENC: 200 cm/s, averages: 2, GRAPPA: 2, temporal resolution: 18.5 ms, acquisition time: 65.2±9.8 s. The real-time perturbed spiral PCMR sequence was acquired with the same trajectory (R~18) as used during training and the following parameters - voxel-size: 1.76x1.76x6.0 mm, FOV: 450x450 mm, Flip Angle: 20^{o}, VENC: 200 cm/s, TR/TE: 6.7/1.9 ms, temporal resolution: ~26.6 ms, acquisition time: ~7.2s.

The real-time perturbed spiral acquisition results in 270 paired flow-encoded and flow-compensated images. Offline U-Net MAE and U-Net SSIM augmented reconstruction was performed on blocks of 96 raw k-space frames with 6 frames of overlap. The reconstructed data was then cropped to keep the central 90 frames in order to remove temporal edge effects due to 3D convolutions. The same raw k-space data also underwent a state-of-the-art CS reconstruction (combining parallel imaging with spatio-temporal total variation regularization as optimized in [4]). Coil sensitivity estimation was performed from temporally averaged k-space center using the Berkeley Advanced Reconstruction Toolbox [16]. Both CS and U-net augmented reconstructions were performed on the same workstation with Windows 10 and an NVIDIA Tesla K40c (12GB Memory) to enable comparison of reconstruction times.

Analysis

All quantitative analyses were carried out by using in-house plug-ins for Horos software (Horos, MD USA).

For flow analysis, the aorta was segmented (GTK - 10 years experience) on the magnitude of the U-Net SSIM, CS and Cartesian images using a semi-automatic method based on the optical flow registration with manual operator correction [17]. The resultant regions of interest (ROI) were transferred to the corresponding phase images (U-Net SSIM based ROIs were also applied to U-Net MAE images) to produce flow and mean velocity curves. Peak mean velocity was taken as the maximum of the mean velocity curve. Stroke volume

(SV) was calculated by integrating the resultant flow curve over a single r-r interval. As multiple heartbeats are evaluated with real-time PCMR, SV and peak velocity were averaged across all complete r-r intervals.

Quantitative edge sharpness was calculated at peak systole by measuring the maximum gradient of the normalized pixel intensities across the aortic wall as previously described [4]. For the real-time data the edge sharpness measurements were performed in all peak systole frames and the averaged values were used for comparisons.

Statistical Analysis

All statistical analysis was performed using R software (R Foundation for Statistical Computing, Vienna, Austria) and a p-value of less than 0.05 indicated a significant difference. All the results are expressed as mean ± standard deviation. Differences between the imaging techniques were assessed using the one-way repeated measures analysis of variance (ANOVA). The imaging techniques were treated as the repeated measures factor. Significant results were further investigated with post-hoc pairwise comparison using the Tukey method.

Results

Synthetic data study

U-Net MAE and U-Net SSIM both had 1,550,818 trainable parameters and took ~6 and ~14 hours to train, respectively (U-Net SSIM was slower due to the additional computation time for the 3D SSIM loss).

Quantitative results are summarized in Table 1. A representative test case showing gridded (input to the network), U-Net MAE, U-Net SSIM and truth images is shown in Figure 2 and Supporting Information Video S1. Both DL networks successfully removed the artifacts from the undersampled input complex-valued images, with an improvement in all image metrics compared to the gridded images. The perturbed spiral consistently

outperformed uniform spiral sampling in synthetic test data for all metrics ($p<0.05$) except phase SSIM where no statistical differences between the two were observed.

The U-Net MAE resulted in lower MAE and higher PSNR, while the U-Net SSIM produced higher average SSIM, magnitude SSIM and phase SSIM. On inspection, U-Net MAE images appeared qualitatively blurrier than the U-Net SSIM ones.

In-vivo study

Representative gridded, U-Net MAE, U-Net SSIM and CS images of prospective real-time data, as well as Cartesian data are shown in Figure 3.A (corresponding movies are shown in Supporting Information Video S2 and Video S3). Separate flow-compensated, flow-encoded, and phase subtracted images that were deep artifact suppressed using U-Net MAE and U-Net SSIM models are shown in Figure 4. It can be seen that both networks were able to suppress artifacts in both flow-encoded, and flow-compensated data. Quantitatively, edge sharpness was lowest in the U-Net MAE images (Table 2) and was significantly lower than both Cartesian ($p<0.0001$) and CS images ($p=0.001$). U-Net SSIM images were less sharp than the Cartesian images ($p=0.002$), but not than the CS images ($p=0.24$).

Representative averaged flow and mean velocity curves are shown in Figure 3.B and Figure 3.C (curves for all heart beats are shown in Supporting Information Figure S1). Quantitative results are summarized in Table 2 and Bland Altman plots comparing SV and peak mean velocities to the Cartesian reference are shown in Figure 5. Stroke volumes from all real-time methods had a small negative bias compared to Cartesian flow, but none reached significance. There were also no significant differences in stroke volume between the real-time methods (Table 2).

Peak mean velocities were significantly lower for the U-Net MAE compared to the Cartesian sequence, due to blurring of the velocity curve (Figure 3.C). There was no significant difference in peak mean velocity between U-Net SSIM, CS real-time data and

reference Cartesian data. However, the limits of agreement with the Cartesian data for both U-Net methods were wider than for CS reconstructions.

The reconstruction of 96 frames took ~59 seconds (0.6s/frame) using CS, while U-Net augmented reconstructions took 3.9 seconds (0.04s/frame, ~15 times faster), which included 0.8 seconds for coil estimation, 1.8 seconds for gridding and FFT of both contrasts and 1.3 seconds for denoising and combining of both contrasts.

Discussion

In this study, we proposed a DL framework for fast artifact suppression of heavily undersampled real-time spiral PCMR data. The main findings were: 1) perturbed spiral trajectories were better suited for the proposed artifact suppression than uniform density spirals, 2) DL networks were able to remove undersampling artifact from prospectively acquired perturbed spiral real-time data, 3) A model trained with a complex SSIM loss produced more accurate flow quantification than complex MAE loss, 4) the DL method was 15 times faster than CS reconstruction enabling better integration in the clinical workflow.

In this study, we focused on U-Net based artifact suppression to remove aliasing artifact from undersampled spiral PCMR data. This approach seems to be reliant on noise-like aliases [8] and therefore we investigated the use of a perturbed spiral trajectory designed to produce incoherent undersampling artifacts. Synthetic perturbed trajectory data produced more accurate images than uniform density spirals (higher SSIM, higher PSNR and lower MAE) and was thus used for the in-vivo study.

We also investigated the use of different loss functions during network training. In previous MR studies, SSIM loss has been extensively used for reconstruction of magnitude images [18–20]. However, to our knowledge the use of SSIM has not been extended to complex-valued problems, where MAE [11,14] or MSE [21] losses are more commonly used. Therefore, we proposed a novel 3D SSIM loss for complex-valued images which

demonstrated higher magnitude and phase SSIM in the synthetic test set, compared to MAE. However, using MAE for training also resulted in lower MAE in the validation set, demonstrating the problem of using the same metric as a loss and measure of image quality. Thus, to determine which loss was better we compared U-Net SSIM, MAE and CS reconstructions of prospective real-time data to reference standard Cartesian flow in children undergoing routine CMR.

Both U-Nets were able to successfully remove aliasing artifacts from prospective 18x undersampled perturbed spiral real-time data (both flow-compensated and flow-encoded images) acquired in free-breathing. This was despite the fact that the network was trained on 1) modified phase subtracted data and 2) breath-hold data suggesting good generalizability. As a result, there were no significant differences in stroke volumes between any of the techniques. However, peak mean velocity was significantly lower for the U-Net MAE images due to temporal blurring of the velocity curve. In addition, the U-Net MAE produced images with the lowest edge sharpness. This implies that the SSIM loss performs better, producing sharper images in both space and time. There were some contrast differences between CS and DL based methods, even though the underlying raw data was the same. This was probably due to differences in the reconstruction framework including coil estimation, normalization of gridded images and data consistency. Learning from multi-coil raw data and including data consistency layers could lead to more consistent images and further improve final results [22].

It should be noted that the limits of agreement between U-Net SSIM and Cartesian measurements were wider than between CS and Cartesian measurements. However, they were similar to previously reported limits of agreement for a standard Cartesian breath hold PCMR that is extensively used in the clinical environment [3]. Furthermore, they are within the range of recently reported scan-scan repeatability [23]. Therefore, we believe that the magnitude of any errors are within the clinically acceptable range. Further improvement may be achieved using other losses such as multiscale SSIM (MS-SSIM) [24] or MAE + MS-SSIM [25] and these will be investigated in future work. The main benefit of our

proposed DL artifact suppression method is that it leverages data routinely stored in clinical archives (magnitude and phase subtracted images, i.e. no raw data). This enabled us to retrospectively collect data from a substantial number of pediatric and congenital heart disease patients (520 cases). Our findings were in line with recent work [11] proposing deep artifact suppression for radial real-time PCMR. The main difference in our study was the use of spiral trajectories, which enabled imaging at higher spatial ($2.0x2.0mm^2$ vs $1.76x1.76mm^2$) and higher temporal (43.1ms vs 26.6ms) resolution [11]. Additionally, we investigated the framework in a specific cohort of patients (i.e. children with heart disease) in whom real-time PCMR is highly desirable.

A hybrid method proposing to use DL for the creation of a high-quality prior for a kt-SENSE reconstruction for real-time PCMR data [26] was recently proposed to provide data consistent reconstructions while speeding up the reconstruction compared to CS (3.6X speed up). The main advantage of our approach over hybrid and CS methods are the shorter reconstruction times, as demonstrated here (15x speed up). This leads to the reconstruction (raw k-space to final phase subtracted images) of 270 frames (7.2 seconds of acquisition) in 11.7 seconds which could help fluidify workflow compared to the 177 seconds needed for CS. This should significantly aid in the dissemination and deployment of novel real-time PCMR sequences into the clinical environment.

Future works will aim at applying a similar method for beat-to-beat monitoring of cardiac output with real-time feedback. The current method will require additional fully automatic segmentation, reduction in latency and online reconstruction. For this purpose, efficient online reconstruction, joint artifact suppression and segmentation [27] and lowering the number of input frames will be investigated.

Conclusion

We have demonstrated that a U-Net based method can successfully remove aliasing artifact from heavily undersampled spiral real-time phase contrast cardiac MR. The proposed U-Net was trained using clinically available DICOMs only and optimized on an adapted

SSIM for complex values. It outperformed the same U-Net with complex MAE loss in a prospective population of 20 pediatric patients with congenital heart disease and enabled fast and accurate flow quantification while significantly reducing reconstruction times.

Acknowledgements: This work was supported by the British Heart Foundation (grant: NH/18/1/33511). JAS and JMT are funded under the UKRI Future Leaders Fellowship (MR/S032290/1). JMT and GTK are also part funded by Heart Research UK (RG2661/17/20).

Figures

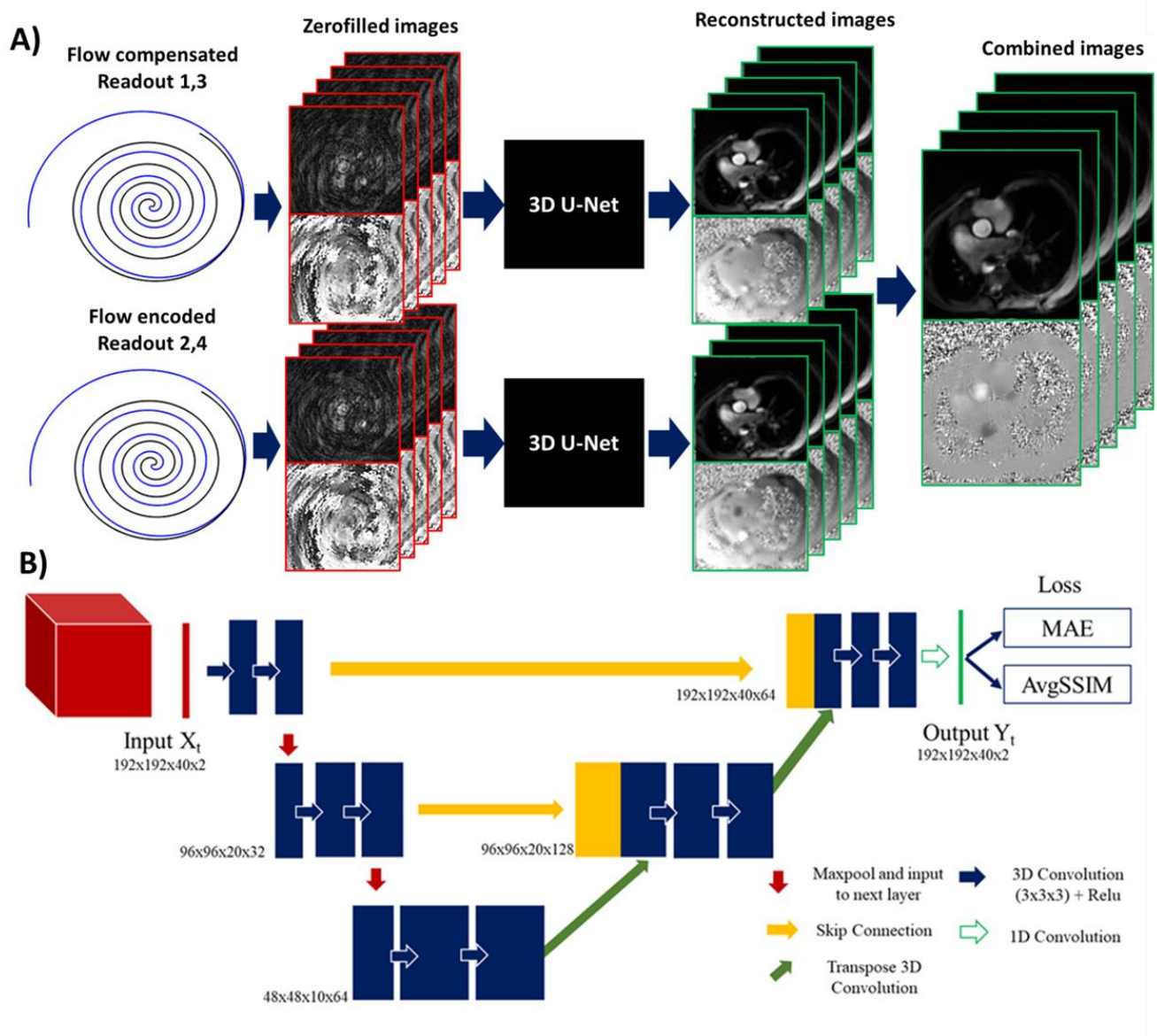

Figure 1. A) Proposed reconstruction of PCMR data acquired with a perturbed spiral trajectory (first four spiral arms shown). Flow-compensated and flow-encoded data are gridded, and Fourier transformed into image space, before being denoised using a 3D U-Net and then combined (average magnitude, phase subtraction) to provide PCMR images. B) U-Net model used for artifact suppression. The real and imaginary are concatenated in the channel dimension leading to a 3D (2D+time) input volume of size 192x192x40x2. Two 3D convolutions are applied at each scale, with three image scales used in both encoding and decoding. The network was trained using either a mean absolute error (MAE) loss or an adapted 3D SSIM loss for complex valued output (AvgSSIM).

Trajectory	Reconstruction	MAE	PSNR	Average SSIM	Magnitude SSIM	Phase SSIM
Uniform Spiral	Gridded	0.1265	15.9	0.45	0.56	0.23
	U-Net MAE	0.0457	24.5	0.85	0.85	0.79
	U-Net SSIM	0.0464	24.3	0.85	0.86	**0.81**
Perturbed Spiral	Gridded	0.1171	16.6	0.47	0.59	0.27
	U-Net MAE	**0.0417***	**25.3***	0.85	0.86	0.79
	U-Net SSIM	0.0448	24.6	**0.86***	**0.88***	**0.81**

Table 1. Results from synthetic test data: Mean absolute error (MAE), Peak Signal to Noise Ratio (PSNR), average SSIM (average of real and imaginary), magnitude SSIM and phase SSIM, obtained in the synthetic test data shown for uniform and perturbed spiral samplings and gridded, U-Net MAE and U-Net SSIM methods. * indicates statistical significance ($p<0.05$) between the best and second best performing methods.

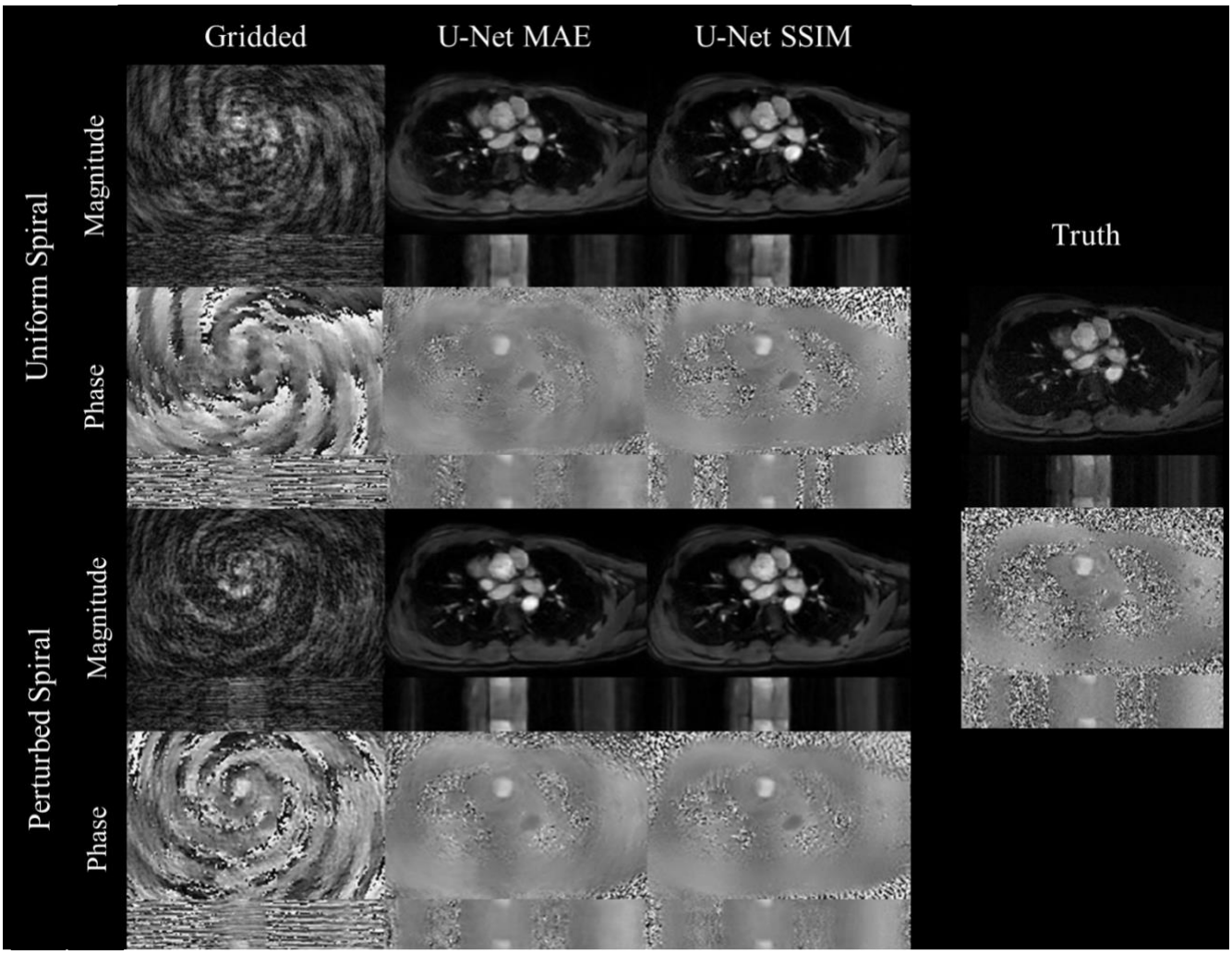

Figure 2. Representative result from the synthetic test cases: Gridded, U-Net MAE and U-Net SSIM images (x-y frame at peak systole and x-t cross-section of the aorta) for uniform spiral (Top) and

perturbed spiral (Bottom) compared to corresponding truth images (far right). U-Net MAE results appear blurrier than U-Net SSIM, (especially phase images) for both trajectories.

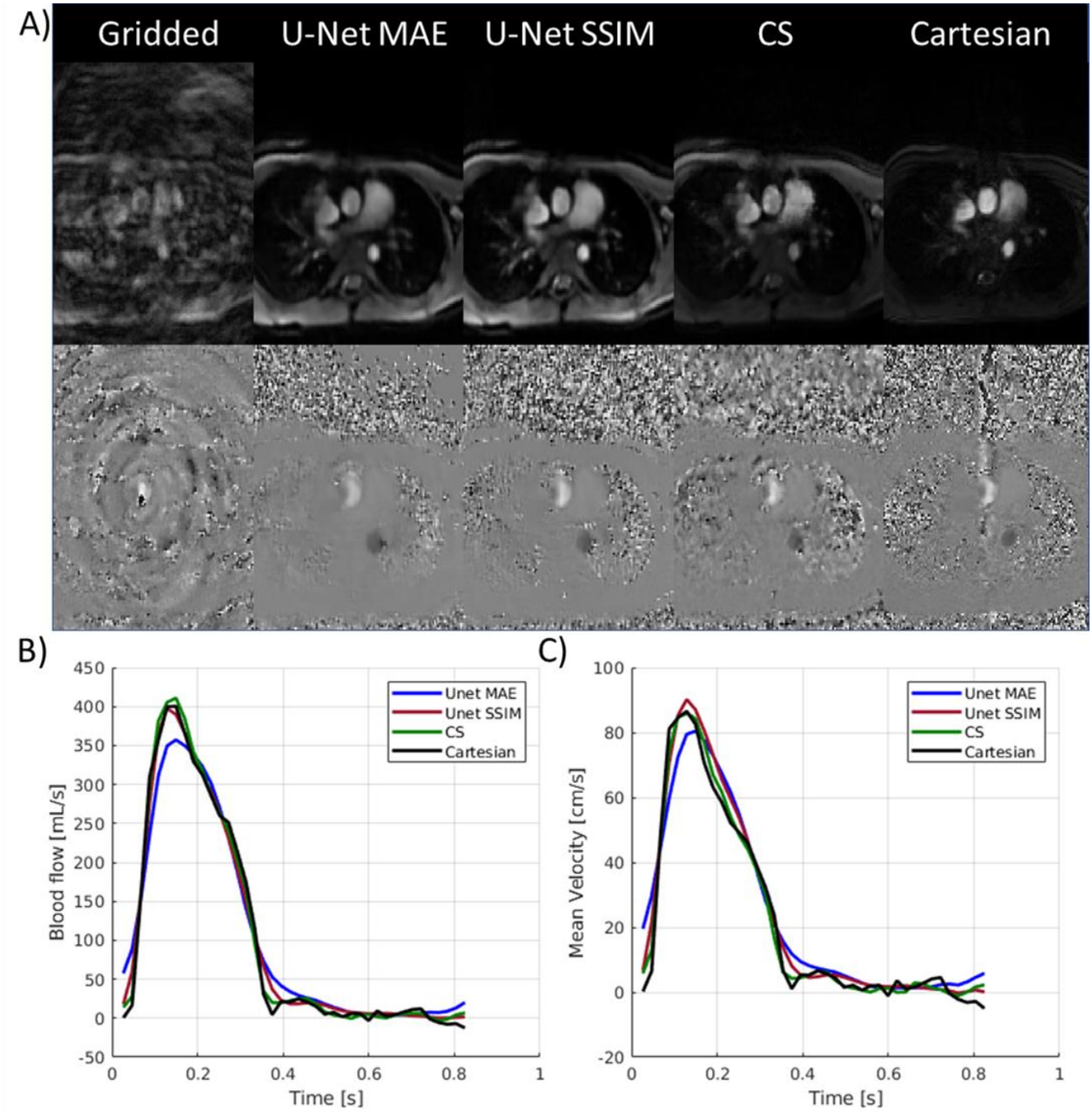

Figure 3. Results from a representative prospectively acquired subject. A) Gridded, U-Net MAE, U-Net SSIM, CS and Cartesian results at peak systole. B) Corresponding average real-time flow curves compared to the Cartesian reference. C) Corresponding average real-time mean velocity curves compared to the Cartesian reference. Corresponding real-time videos can be found in Supporting Information Video S2

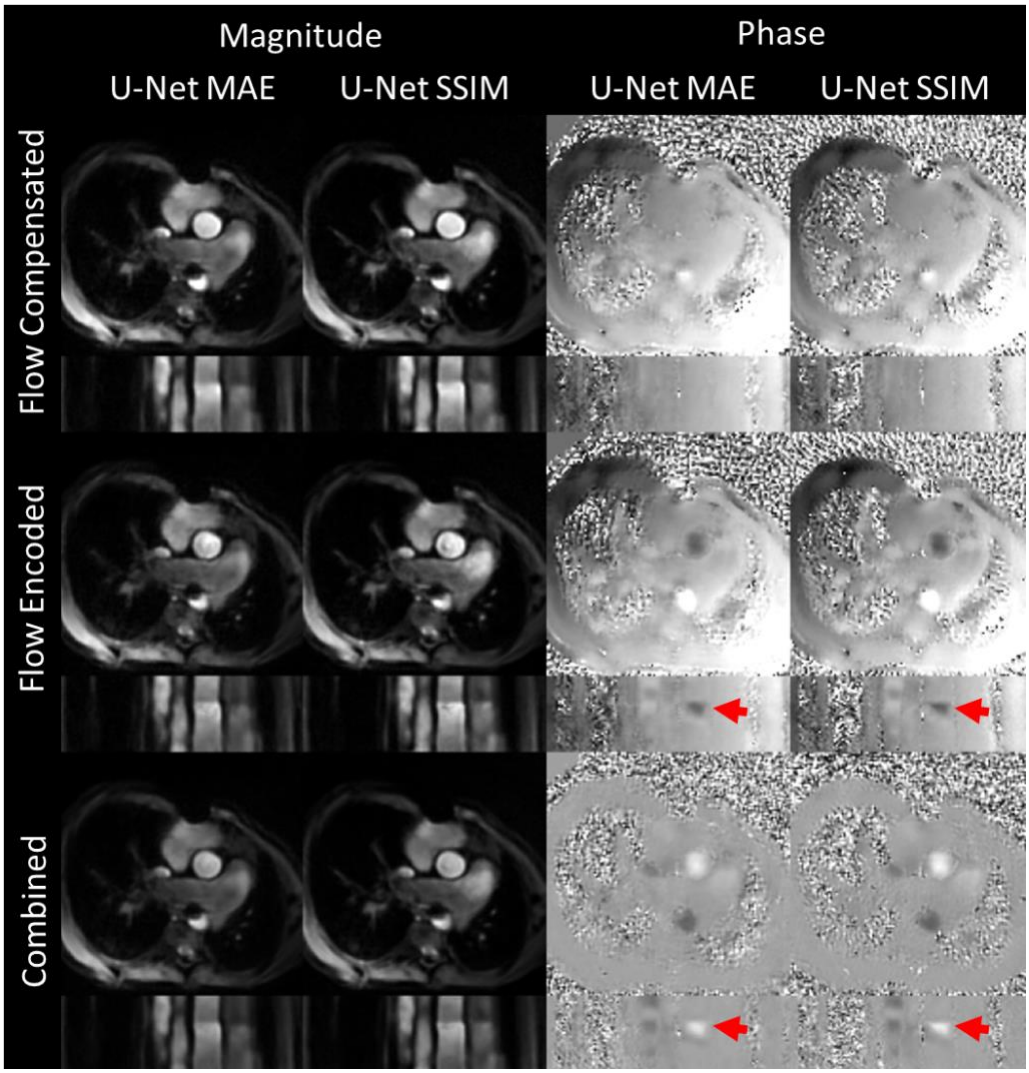

Figure 4. Prospective images from one patient. Flow-compensated, flow-encoded and PCMR combined images (x-y frame at peak systole and x-t cross-section of the aorta) for U-Net MAE and U-Net SSIM. Phase images appear sharper using U-Net SSIM (as depicted by the red arrow).

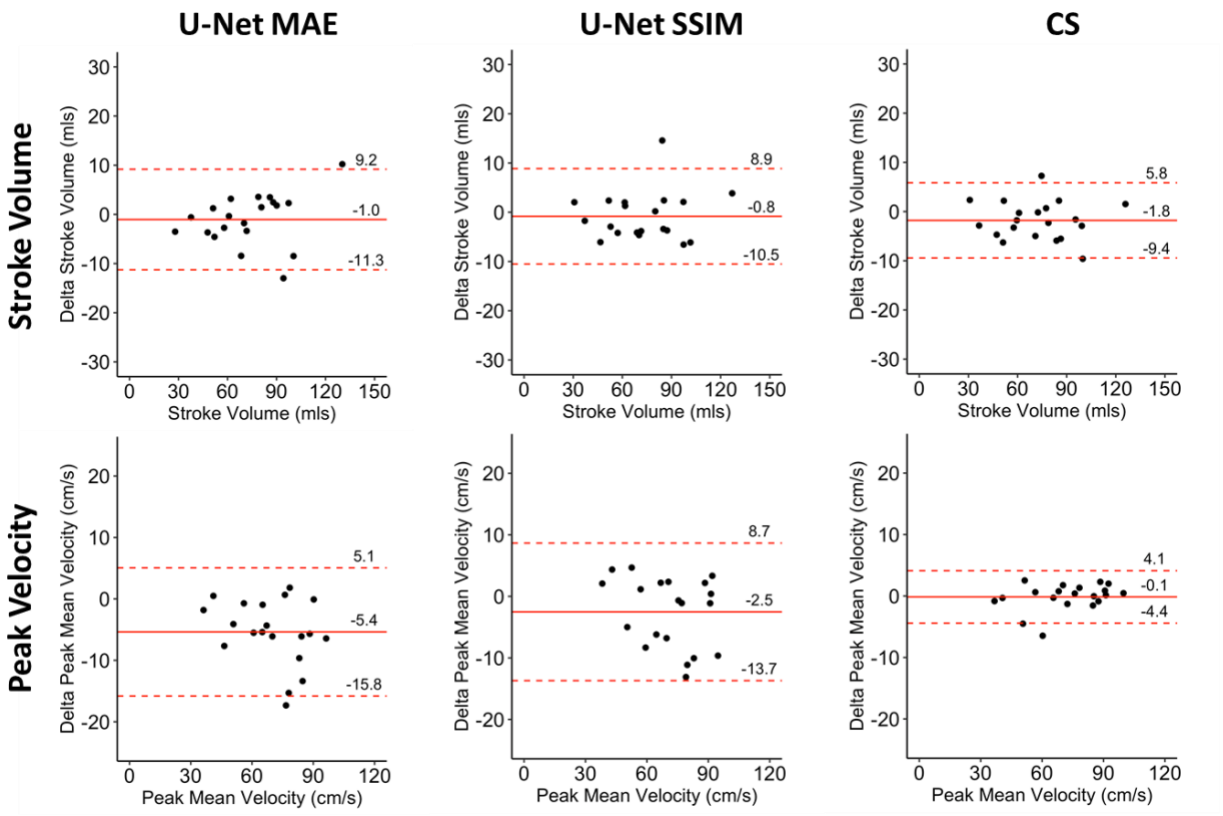

Figure 5. Bland Altmann plots comparing U-Net MAE, U-Net SSIM and CS to reference Cartesian stroke volume (Top) and peak mean velocity (Bottom).

	U-Net MAE	U-Net SSIM	CS	Cartesian
Stroke Volume ± std (mL)	72.1±25.1	72.4±24.2	71.4±23.4	73.2±23.7
Bias (mL) [Limits of Agreement]	-1.0 [-11.3; 9.2]	-0.8 [-10.5; 8.9]	-1.8 [-9.4; 5.8]	N/A
Peak Mean Velocity ± std (cm/s)	67.0*±16.4	69.9±16.4	72.3±18.6	72.4±18.0
Bias (cm/s) [Limits of Agreement]	-5.4* [-15.8; 5.1]	-2.5 [-13.7; 8.7]	-0.1 [-4.4; 4.1]	N/A
Edge Sharpness	0.083*±0.026	0.101*±0.034	0.119±0.037	0.136±0.033
Recon. time (96 frames)	~3.9s	~3.9s	~59s	N/A

* indicates statistically significant ($p<0.05$) differences compared to Cartesian

Table 2. Table summarizing prospective in-vivo measurements. Average values, standard deviation (std), biases and limits of agreements (LOA) for stroke volume and peak mean velocity are reported. Edge sharpness and reconstruction times for the different methods are also reported. * indicates statistically significant differences ($p<0.05$) with reference Cartesian measurements.

Supporting Information Figures

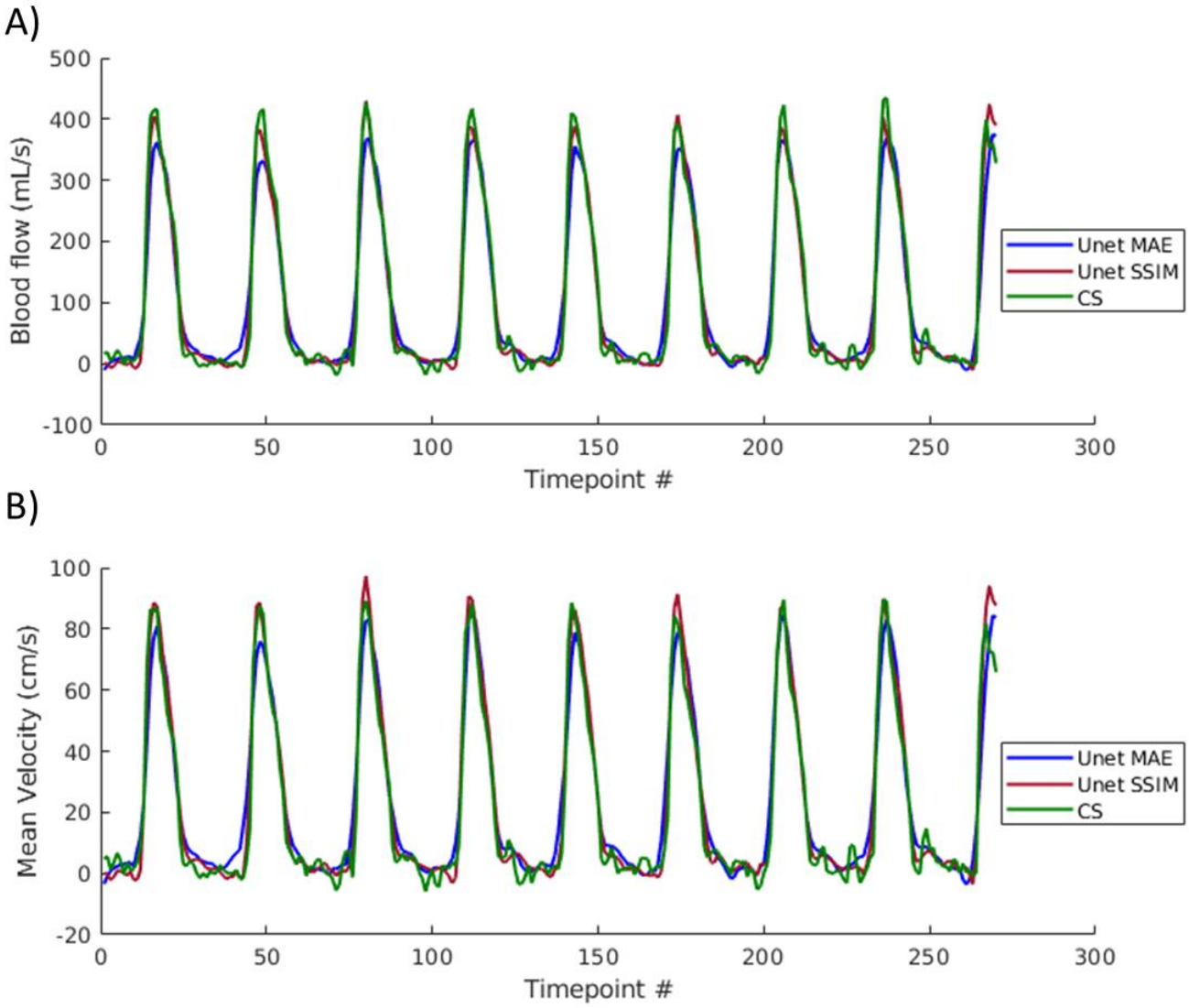

Supporting Information Figure S1. Representative flow analysis from one prospective real-time data set A) flow and B) mean velocity curves acquired over ~7.2 seconds and reconstructed using U-Net MAE, U-Net SSIM and Compressed Sensing (CS). Corresponding images are shown in Supporting Information Video S2.

Supporting Information Video S1. Simulated gridded, U-Net MAE, U-Net SSIM reconstructions for uniform spiral (Top) and perturbed spiral (Bottom) compared to corresponding truth images (utmost right).

Supporting Information Video S2. Gridded, U-Net MAE, U-Net SSIM and CS combined flow images in a representative prospectively acquired subject. Corresponding real-time flow and mean velocity curves are shown in Supporting Information Figure S1. Corresponding average curves are shown in Figure 3.

Supporting Information Video S3. Gridded, U-Net MAE, U-Net SSIM and CS combined flow images in an additional representative prospectively acquired subject.

References

[1] Firmin DN, Nayler GL, Klipstein RH, Underwood SR, Rees RS, Longmore DB. In vivo validation of MR velocity imaging. J Comput Assist Tomogr 1987;11:751–6. https://doi.org/10.1097/00004728-198709000-00001.

[2] Gatehouse PD, Firmin DN, Collins S, Longmore DB. Real time blood flow imaging by spiral scan phase velocity mapping. Magn Reson Med 1994;31:504–12. https://doi.org/10.1002/mrm.1910310506.

[3] Steeden JA, Atkinson D, Hansen MS, Taylor AM, Muthurangu V. Rapid flow assessment of congenital heart disease with high-spatiotemporal- resolution gated spiral phase-contrast MR imaging. Radiology 2011;260:79–87. https://doi.org/10.1148/radiol.11101844.

[4] Kowalik GT, Knight D, Steeden JA, Muthurangu V. Perturbed spiral real-time phase-contrast MR with compressive sensing reconstruction for assessment of flow in children. Magn Reson Med 2020;83:2077–91. https://doi.org/10.1002/mrm.28065.

[5] Lustig M, Donoho D, Pauly JM. Sparse MRI: The application of compressed sensing for rapid MR imaging. Magn Reson Med 2007;58:1182–95. https://doi.org/10.1002/mrm.21391.

[6] Haji-Valizadeh H, Feng L, Ma LE, Shen D, Block KT, Robinson JD, et al. Highly

accelerated, real-time phase-contrast MRI using radial k-space sampling and GROG-GRASP reconstruction: a feasibility study in pediatric patients with congenital heart disease. NMR Biomed 2020;33:e4240. https://doi.org/10.1002/nbm.4240.

[7] Bustin A, Fuin N, Botnar RM, Prieto C. From Compressed-Sensing to Artificial Intelligence-Based Cardiac MRI Reconstruction. Front Cardiovasc Med 2020;7:17. https://doi.org/10.3389/fcvm.2020.00017.

[8] Hauptmann A, Arridge S, Lucka F, Muthurangu V, Steeden JA. Real-time cardiovascular MR with spatio-temporal artifact suppression using deep learning–proof of concept in congenital heart disease. Magn Reson Med 2019;81:1143–56. https://doi.org/10.1002/mrm.27480.

[9] Schlemper J, Caballero J, Hajnal J V., Price AN, Rueckert D. A Deep Cascade of Convolutional Neural Networks for Dynamic MR Image Reconstruction. IEEE Trans Med Imaging 2018;37:491–503. https://doi.org/10.1109/TMI.2017.2760978.

[10] Hammernik K, Klatzer T, Kobler E, Recht MP, Sodickson DK, Pock T, et al. Learning a variational network for reconstruction of accelerated MRI data. Magn Reson Med 2018;79:3055–71. https://doi.org/10.1002/mrm.26977.

[11] Haji-Valizadeh H, Guo R, Kucukseymen S, Paskavitz A, Cai X, Rodriguez J, et al. Highly accelerated free-breathing real-time phase contrast cardiovascular MRI via complex-difference deep learning. Magn Reson Med 2021;00:mrm.28750. https://doi.org/10.1002/mrm.28750.

[12] Ronneberger O, Fischer P, Brox T. U-net: Convolutional networks for biomedical image segmentation. Lect. Notes Comput. Sci. (including Subser. Lect. Notes Artif. Intell. Lect. Notes Bioinformatics), vol. 9351, Springer Verlag; 2015, p. 234–41. https://doi.org/10.1007/978-3-319-24574-4_28.

[13] Kingma DP, Ba JL. Adam: A method for stochastic optimization. 3rd Int. Conf.

Learn. Represent. ICLR 2015 - Conf. Track Proc., International Conference on Learning Representations, ICLR; 2015.

[14] Cole E, Cheng J, Pauly J, Vasanawala S. Analysis of deep complex-valued convolutional neural networks for MRI reconstruction and phase-focused applications. Magn Reson Med 2021:mrm.28733. https://doi.org/10.1002/mrm.28733.

[15] Wang Z, Bovik AC, Sheikh HR, Simoncelli EP. Image quality assessment: From error visibility to structural similarity. IEEE Trans Image Process 2004;13:600–12. https://doi.org/10.1109/TIP.2003.819861.

[16] Uecker M, Ong F, Tamir JI, Bahri D, Virtue P, Cheng J, et al. Berkeley Advanced Reconstruction Toolbox. Annu Meet ISMRM, Toronto 2015 2015;23:2486.

[17] Odille F, Steeden JA, Muthurangu V, Atkinson D. Automatic segmentation propagation of the aorta in real-time phase contrast MRI using nonrigid registration. J Magn Reson Imaging 2011;33:232–8. https://doi.org/10.1002/jmri.22402.

[18] Sriram A, Zbontar J, Murrell T, Defazio A, Zitnick CL, Yakubova N, et al. End-to-End Variational Networks for Accelerated MRI Reconstruction. ArXiv 2020:2004.06688v2.

[19] Putzky P, Karkalousos D, Teuwen J, Miriakov N, Bakker B, Caan M, et al. i-RIM applied to the fastMRI challenge. ArXiv 2019:1910.08952v1.

[20] Muckley MJ, Riemenschneider B, Radmanesh A, Kim S, Jeong G, Ko J, et al. State-of-the-Art Machine Learning MRI Reconstruction in 2020: Results of the Second fastMRI Challenge. ArXiv 2020:2012.06318v2.

[21] Trabelsi C, Bilaniuk O, Zhang Y, Serdyuk D, Subramanian S, Santos JF, et al. Deep Complex Networks. 6th Int Conf Learn Represent ICLR 2018 - Conf Track Proc 2017.

[22] Hammernik K, Schlemper J, Qin C, Duan J, Summers RM, Rueckert D. Σ-net: Systematic Evaluation of Iterative Deep Neural Networks for Fast Parallel MR Image Reconstruction. ArXiv 2019:1912.09278v1.

[23] Arar Y, Hussain T, Abou Zahr R, Gooty V, Greer JS, Huang R, et al. Fick versus flow: a real-time invasive cardiovascular magnetic resonance (iCMR) reproducibility study. J Cardiovasc Magn Reson 2021 231 2021;23:1–11. https://doi.org/10.1186/S12968-021-00784-7.

[24] Wang Z, Simoncelli EP, Bovik AC. Multi-scale structural similarity for image quality assessment. Conf. Rec. Asilomar Conf. Signals, Syst. Comput., vol. 2, 2003, p. 1398–402. https://doi.org/10.1109/acssc.2003.1292216.

[25] Zhao H, Gallo O, Frosio I, Kautz J. Loss Functions for Image Restoration with Neural Networks. ArXiv 2018:1511.08861v3.

[26] Kowalik GT, Montalt-Tordera J, Steeden J, Muthurangu V, Grzegorz D, Kowalik T. Machine Learning aided k-t SENSE for fast reconstruction of highly accelerated PCMR data. ArXiv 2021:2103.07541.

[27] Buchholz T-O, Prakash M, Krull A, Jug F. DenoiSeg: Joint Denoising and Segmentation. ArXiv 2020:2005.02987v2.